

Integrator based on current-controlled magnetic domain wall

Cite as: Appl. Phys. Lett. **118**, 052402 (2021); <https://doi.org/10.1063/5.0041362>

Submitted: 22 December 2020 • Accepted: 18 January 2021 • Published Online: 01 February 2021

Shijiang Luo, Weicheng Tian, Shuai Zhang, et al.



View Online



Export Citation



CrossMark

ARTICLES YOU MAY BE INTERESTED IN

[Power and area efficient stochastic artificial neural networks using spin-orbit torque-based true random number generator](#)

Applied Physics Letters **118**, 052401 (2021); <https://doi.org/10.1063/5.0035857>

[Spin-orbit torques: Materials, physics, and devices](#)

Applied Physics Letters **118**, 120502 (2021); <https://doi.org/10.1063/5.0039147>

[Field-free and sub-ns magnetization switching of magnetic tunnel junctions by combining spin-transfer torque and spin-orbit torque](#)

Applied Physics Letters **118**, 092406 (2021); <https://doi.org/10.1063/5.0039061>

Time to get excited.
Lock-in Amplifiers – from DC to 8.5 GHz

[Find out more](#)

Zurich Instruments

Integrator based on current-controlled magnetic domain wall

Cite as: Appl. Phys. Lett. **118**, 052402 (2021); doi: [10.1063/5.0041362](https://doi.org/10.1063/5.0041362)

Submitted: 22 December 2020 · Accepted: 18 January 2021 ·

Published Online: 1 February 2021





View Online



Export Citation



CrossMark

Shijiang Luo,¹ Weicheng Tian,¹ Shuai Zhang,¹ Ruofan Li,¹ Run Min,¹ Xiaofei Yang,¹ Xuecheng Zou,¹ Jeongmin Hong,¹  and Long You^{1,2,a)} 

AFFILIATIONS

¹School of Optical and Electronic Information, Huazhong University of Science and Technology, Wuhan 430074, China

²Wuhan National Lab for Optoelectronics, Huazhong University of Science and Technology, Wuhan 430074, China

^{a)} Author to whom correspondence should be addressed: lyou@hust.edu.cn

ABSTRACT

Integrators are widely used in industrial controls, signal processing, and computing. However, traditional resistor–capacitor integrators incur leakage errors and zero drift, hindering their accuracy. By contrast, spintronic devices with good scalability and endurance for memory and logic applications in digital circuits have yet to be studied for analog circuit elements. Here, we propose a single-device spintronic integrator based on the current-controlled magnetic domain wall (DW). Continuous DW motion and correlated changes in the anomalous Hall resistance (or magneto-resistance) are encoded as an analog output signal, which is modulated by an input current through the spin–orbit–torque effect. Waveform transformation and phase-shift functions are demonstrated using Hall-bar devices. The spintronic integrator could pave the way for the spin-based analog computing with high reliability, high endurance, and good compatibility with the CMOS process.

Published under license by AIP Publishing. <https://doi.org/10.1063/5.0041362>

An integrator is an electronic component used to accomplish mathematical operations of calculus functions of integration for shaping different waveforms. Integrators are used in numerous areas of electronics, including electronic analog computers, wave-shaping circuits, and frequency modulators, as well as playing the role of neuromorphic neurons in neural networks.^{1–3} Conventional integrators are fabricated using active operational amplifiers (op-amps) or using passive resistor–capacitor (RC) combinations, the integrating functions of which are realized through a capacitor charge and discharge. However, capacitors incur an intrinsic dielectric loss and leakage resistance, resulting in a nonlinear drift.⁴ Op-amps have an offset current, thereby introducing zero drift.⁵ To eliminate these inherent drawbacks, a conventional RC integrator should be replaced by a more advanced design.

Spin orbit torque (SOT) has attracted significant attention as an alternative way to manipulate the magnetization in a heavy-metal/ferromagnetic (HM/FM) bilayer.^{6–21} A typical SOT device consists of an HM layer, an FM free layer (FL), a nonmagnetic barrier layer (BL), and an FM pinned layer (PL). Among them, FL/BL/PL constitutes a classical sandwich structure, i.e., a magnetic tunneling junction (MTJ), in which the magnetization of the PL remains unchanged, whereas that of the FL can be changed through SOT. For an FL with a single domain, the SOT can switch the magnetization between the upward

and downward directions, which is used in a binary-state SOT-Magnetic Random Access Memory (MRAM).^{22,23} For an FL with dual or multiple domains separated by domain walls (DWs), SOT-induced DW motion can continuously tune the magneto-resistance (MR), which shows memristive behavior.^{24,25} The three-terminal structure of SOT devices offers the advantage of decoupled writing (or programming) and reading (transmission) current paths, thereby leading to unlimited endurance for memory and synapse application,^{26,27} as well as low energy consumption and favorable CMOS compatibility due to controlling electron spins in magnetic devices. If we consider writing current and reading resistance (or voltage) in the SOT device as input and output signals, respectively, an analog operation circuit is possible to be achieved from an SOT device as there is a logical relationship between the writing current and reading resistance.

Here, we experimentally describe the basic working principle of a current-controlled magnetic DW integrator via SOT, to address issues in the conventional RC integrator, the fundamental building block of analog computer. The output signal is encoded through DW motion-induced resistance modulation controlled by the input current signal through the SOT effect. Such a spintronic integrator utilizes a single SOT device without the need for a capacitor, which simplifies the circuit complexity and effectively eliminates intrinsic errors.

Figure 1 shows the concept of a spintronic integrator based on the current-controlled magnetic DW (see the circuit schematics in the [supplementary material](#), Sec. 1). When applying the input voltage (V_{in}) to produce the write current (I_w) flowing through the HM layer, a DW in the FL moves under a current-induced SOT with a velocity (v) having a linear (or quasi-linear) relationship with I_w ^{28–32} (see simulation results in the [supplementary material](#), Sec. 2), that is,

$$I_w = \frac{V_{in}}{R_{HM}}, \quad (1)$$

$$v \sim kI_w, \quad (2)$$

where R_{HM} is the resistance of the HM layer and k is the proportionality coefficient. The distance (s) of the DW motion is equal to the integration of the velocity over time (t), as indicated in the following:

$$s = \int_0^t v(t) dt. \quad (3)$$

The MTJ resistance (R) is linear with s as follows:

$$R(s) = (R_{MAX} - R_{MIN}) \frac{s}{l} + R_{MIN}, \quad (4)$$

with the boundary conditions

$$\begin{aligned} s = 0, R &= R_{MIN}, \\ s = l, R &= R_{MAX}, \end{aligned} \quad (5)$$

where R_{MAX} , R_{MIN} , and l are the maximum resistance, the minimum resistance, and the FL length, respectively. When applying a read current (I_r) vertically through the MTJ, the output voltage (V_{out}) is sensed as follows:

$$V_{out} = I_r R. \quad (6)$$

Hence, the V_{out} - V_{in} integral relation is built in the following manner:

$$V_{out} = a \int_0^t V_{in}(t) dt + b, \quad (7)$$

$$a = \frac{kI_r(R_{MAX} - R_{MIN})}{lR_{HM}}, \quad (8)$$

thus implementing the integrating function.

As a proof-of-concept, Hall-bar devices, which can be extended to an MTJ structure, were fabricated from a stack of thermally oxidized Si (substrate)/Ta (5 nm)/CoFeB (1.3 nm)/MgO (1 nm)/Ta (1 nm) using a standard etching process including photolithography and ion milling techniques. Figure 2(a) shows the measurement setup along with the definition of the x - y - z coordinates and an optical microscope image of the device. Anomalous Hall effect (AHE) resistance (R_H) measurements were conducted to identify the DW motion. R_H is proportional to M_x and is recorded by applying a read current along the x -direction and detecting the Hall voltage in the y -direction.

Figure 2(b) shows a typical AHE loop (R_H vs out-of-plane field H_z), indicating a strong perpendicular magnetic anisotropy. The current-induced SOT switching of the magnetization is depicted as an R_H - I_w loop under an in-plane field $H_x = 50$ Oe, as shown in Fig. 2(c). The reversal of the magnetization shows a continuous transition with intermediate states rather than an abrupt switching, indicating the memristive behavior originating from the quasi-continuous DW motion.²⁴

We then investigated a train of current pulse-induced gradual AHE resistance modulation (ΔR_H) under different current amplitudes [Fig. 2(d)]. The width of each pulse is 50 μ s. Starting from a saturated downward magnetization state, the input current generates a reversed domain at the left edge of the Hall bar. For practical application, DW nucleation sites can be designated in a well-defined region by the stray field,³³ Oersted field,³⁴ or anisotropy variation engineering.³⁵ Before each measurement, the DW was initially located at the same position and then moved forward along the x -direction under the current pulses through the SOT as long as the current amplitude exceeded the critical current of the DW depinning ($I_c = \sim 29$ mA for our devices, see the [supplementary material](#), Sec. 3). When $I_w > I_c$, R_H increases linearly over time during the first stage. A larger I_w leads to a larger slope of the ΔR_H variation, corresponding to a higher DW velocity. Moreover, a nonlinear region exists for a large I_w (e.g., 33 mA) when R_H approaches saturation. This might originate from the tilted DW approaching the boundary.^{24,36,37} If the FL is sufficiently long, the nonlinear region can be eliminated.

In addition to the current amplitude, the magnitude of the magnetic field also has an effect on the DW velocity and, thus, the resistance modulation, as shown in Fig. 2(e). For a practical application, however, integrating a magnetic field into a device is not desirable. To

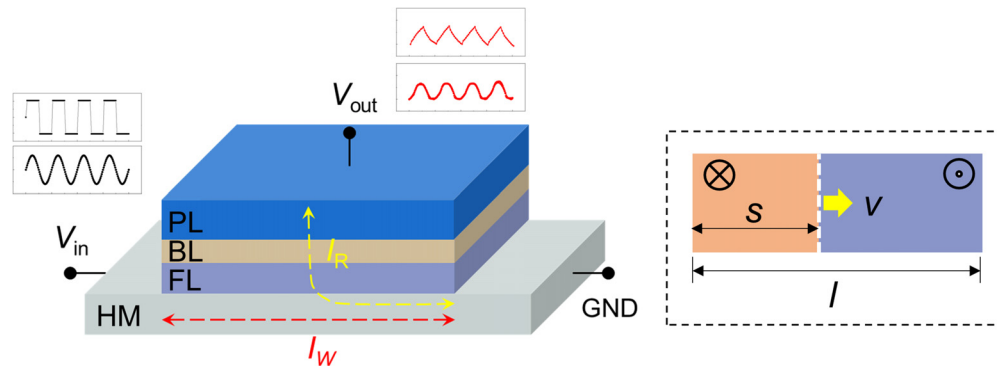


FIG. 1. Schematic of the integrator based on the current-controlled magnetic domain wall. Input voltage (V_{in}) producing the write current (I_w), which flows through the HM layer, to move the domain wall in the FL layer through the SOT. A read current (I_r) vertically flowing through the MTJ to read out the MR, sensing the output voltage (V_{out}).

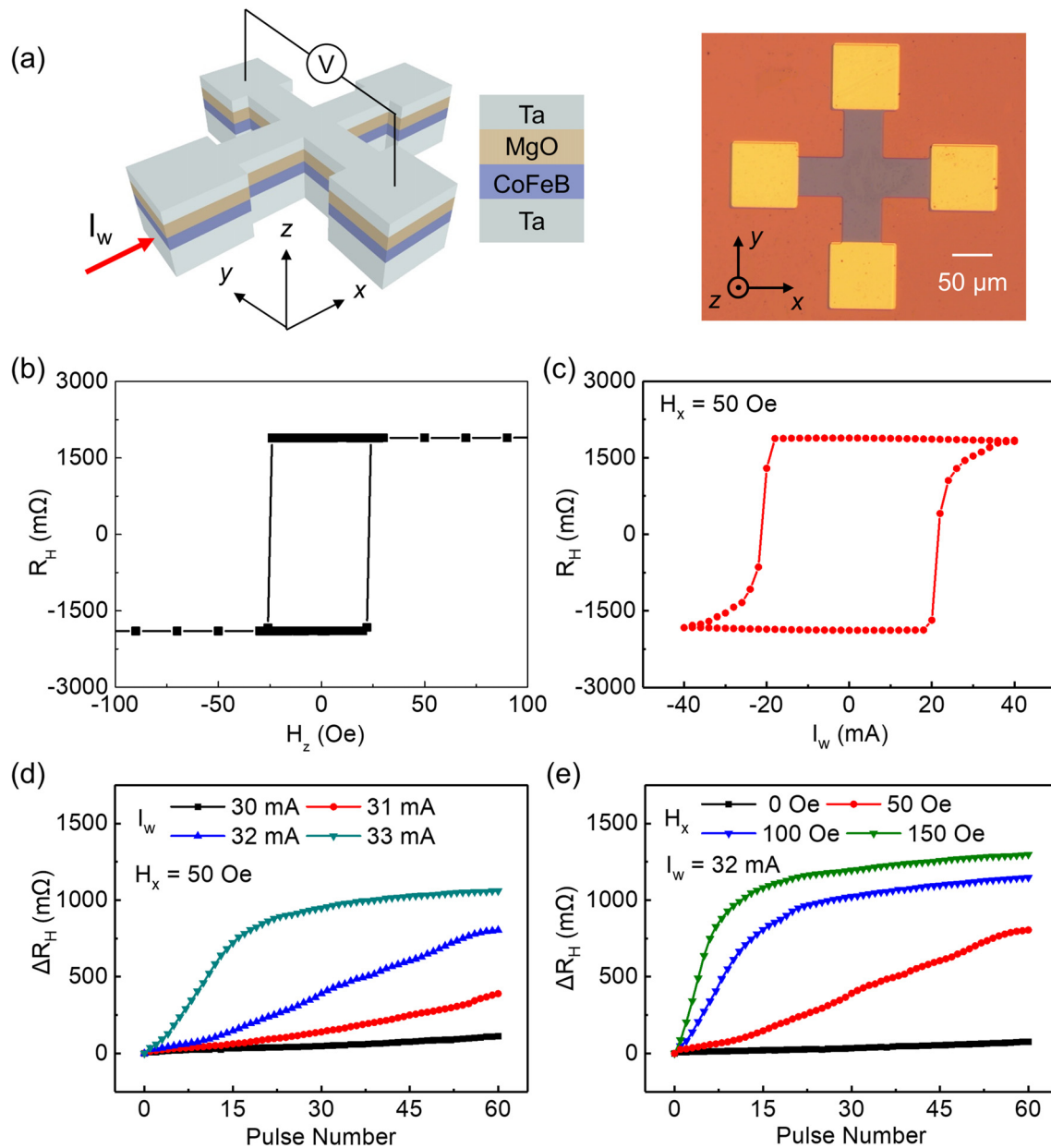


FIG. 2. Integrator based on a Hall bar device with Ta/CoFeB/MgO heterostructures. (a) Device structure with a schematic of the measurement setup (left) and an optical microscope image (right). (b) AHE resistance (R_H) as a function of the out-of-plane magnetic field (H_z). (c) Current-induced R_H switching under an in-plane magnetic field $H_x = +50 \text{ Oe}$. (d) and (e) R_H variation (ΔR_H) modulated by consecutive current pulses under different I_w (d) and H_x (e) values.

further realize a field-free SOT-driven DW motion, one of the approaches is to use a magnetic material system with a chiral DW.³⁸

Next, input-output characteristic measurements were conducted to verify the integrating function of our devices. Here, the input signal is an I_w protocol along with a fixed H_x value of 50 Oe , and the output is ΔR_H . We first select a square waveform with an amplitude of $I_{\text{amp}} = 32 \text{ mA}$ (corresponding to a voltage of $\sim 4.5 \text{ V}$, see the [supplementary material](#), Sec. 4) and a period of $T = 1 \text{ ms}$ as the input. The current pulses with an alternating polarity drive the DW forward and

backward along the x -direction, corresponding to an increase and decrease in ΔR_H , respectively, as shown in Fig. 3(a). As a result, the evolution of ΔR_H shows a triangular shape with the same period as the input waveform. Thus, a waveform transformation from a square to a triangle wave is realized, which is one of the most basic functions of an integrator.

By rationally increasing I_{amp} , the changes in ΔR_H correspondingly increase, as shown in Fig. 3(b). A larger I_{amp} leads to a higher DW velocity and, thus, a longer distance of motion within a one-half

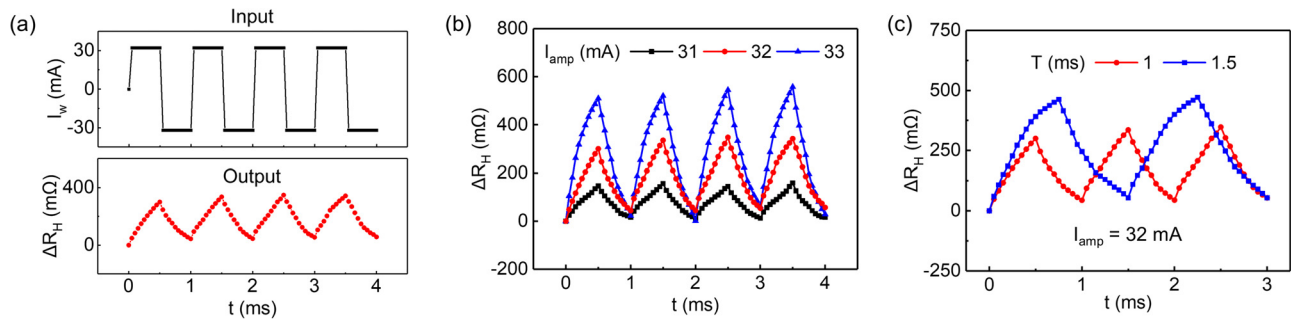


FIG. 3. Input–output characteristic measurements of square waveform input. (a) Input current of the square waveform and corresponding output of ΔR_H showing a triangle waveform. (b) and (c) ΔR_H outputs under square waveform inputs with different I_{amp} (b) and T (c) values.

period. Furthermore, at a large I_{amp} [e.g., 33 mA, as shown in the blue curve in Fig. 3(b)], the output waveform becomes a sawtooth wave instead of a triangular wave owing to the presence of a nonlinear region, as mentioned above. If given an extremely large I_{amp} (not shown), the DW will move quickly and reach the boundary within a one-half period, corresponding to R_H quickly reaching a limit value (i.e., R_{MAX}). In addition, square wave inputs with a different T were also studied. Similar triangle waveform outputs were obtained. As T increases, larger changes in ΔR_H were also acquired.

In addition to a square-to-triangle/sawtooth waveform transformation, commonly used integrators can also transfer a sine waveform into a cosine waveform, which implements a phase shift function. A sine waveform of $I = I_{amp} \cdot \sin(2\pi t/T)$ is applied in our devices. Figure 4(a) shows the input of $I_{amp} = 32$ mA and $T = 2$ ms. The corresponding output signal presents a ladder-like waveform rather than a cosine waveform. This visible distortion is due to the presence of I_c . The DW can be driven to move under the SOT only when I_w exceeds I_c . Therefore, R_H remains unchanged for the stages of $I_w < I_c$ during a sinusoidal input. To solve this problem, we introduce an assisted bias current (I_{bias}) with a square waveform of amplitude $I_{bias,amp} = I_c$ superimposed on the sinusoidal input, enabling an uninterrupted DW motion. Figure 4(b) shows the input of $I_{bias,amp} = 29$ mA, $I_{amp} = 4$ mA, and $T = 2$ ms. Consequently, the output shows a cosine waveform with a phase shift of $\sim 90^\circ$ as compared to the input sine waveform. Sinusoidal inputs with different I_{amp} and T values were also investigated to guarantee the robustness, as shown in Figs. 4(c) and 4(d). The corresponding outputs are stable cosine waveforms with different changes in ΔR_H . This phenomenon is similar to that of the square input counterparts. Hence, a sine-to-cosine waveform transformation and a phase shift, with an adjustable sensing margin and frequency, were realized based on a spintronic integrator.

A time constant (τ) is a critical merit of an integrator. In general, a large τ is required to ensure the integration. As compared to $\tau = RC$ for an RC integrator, the value of τ for a spintronic integrator is determined by l/k , which is related to the effective time of DW motion in the length direction. To increase τ , we can simply increase l . Besides, a material system with a smaller k (i.e., a smaller v under the same I_w) is preferred. A signal gain is a merit of the ability to increase the signal amplitude or power from the input to the output. The signal gain of an integrator is related to the integral coefficient (a). For an RC integrator, $a = 1/RC$, which is fixed after the manufacturing process. By contrast, the value of a for a spintronic integrator is expressed through

Eq. (8), in which the variable I_r can be adjusted even after the device fabrication, significantly enhancing the flexibility to tune the output voltage amplitude. Furthermore, to improve the signal gain at higher frequency, the material systems with larger velocity of DW motion are preferred, so that the DW can move in a larger distance range and, thereby, a larger variation of output signal within a certain period. The DW velocity of up to 750 m/s driven by exchange-coupling torque in synthetic antiferromagnets has been observed,³⁰ corresponding to a working frequency of GHz in a hundred-nm-sized integrator.

Owing to the offset current of the active op-amp, the output signal of the RC integrator deviates from the original value even without an input signal, which is known as zero drift.⁵ As the integration time increases, the integration error continues to accumulate, which leads to a reduction in accuracy. In practical application, to ensure the high accuracy, the RC integrator system needs to include integrator module/circuit along with an extra control module/circuit. Many other devices, such as analog-to-digital converter (ADC)-register-digital-to-analog converter (DAC) and digital signal processor (DSP),⁵ are used for drift compensation, which cost a large chip area. For a spintronic integrator, an op-amp would be connected to the output path, and its offset current does not flow to the input path. Therefore, the output signal only changes with the advent of the effective input signal, and hence, no zero drift occurs. However, due to the stochastic property of current-induced DW motion, the output waveforms differ from cycle to cycle and period to period (see the supplementary material, Sec. 5). Therefore, the accuracy of spintronic integrators mainly depends on the stability of current-induced DW motion, which can be further improved by optimizing the material preparation/device fabrication. Besides, to ensure the integrator functionality, the SOT device with the domain wall cannot be too small. The spintronic integrator device is expected to be further scaled down to a nanowire structure with hundreds-of-nm length³³ and sub-100-nm width.³⁶

The Ta/CoFeB/MgO heterostructure used in a spintronic integrator is compatible with the CMOS process and commonly used in a commercial MRAM product. The high endurance of a CoFeB magnet has been widely reported, and similar to our integrator device based on the DW motion, a DW-motion MRAM with a CoFeB magnet remains extremely stable after 10^{10} writing cycles.³³ The use of the spintronic integrator is a promising way to achieve a high endurance.

In summary, we have proposed a spintronic integrator based on input-current modulated DW motion and, thus, an output resistance signal through an SOT. Input-output measurement results have

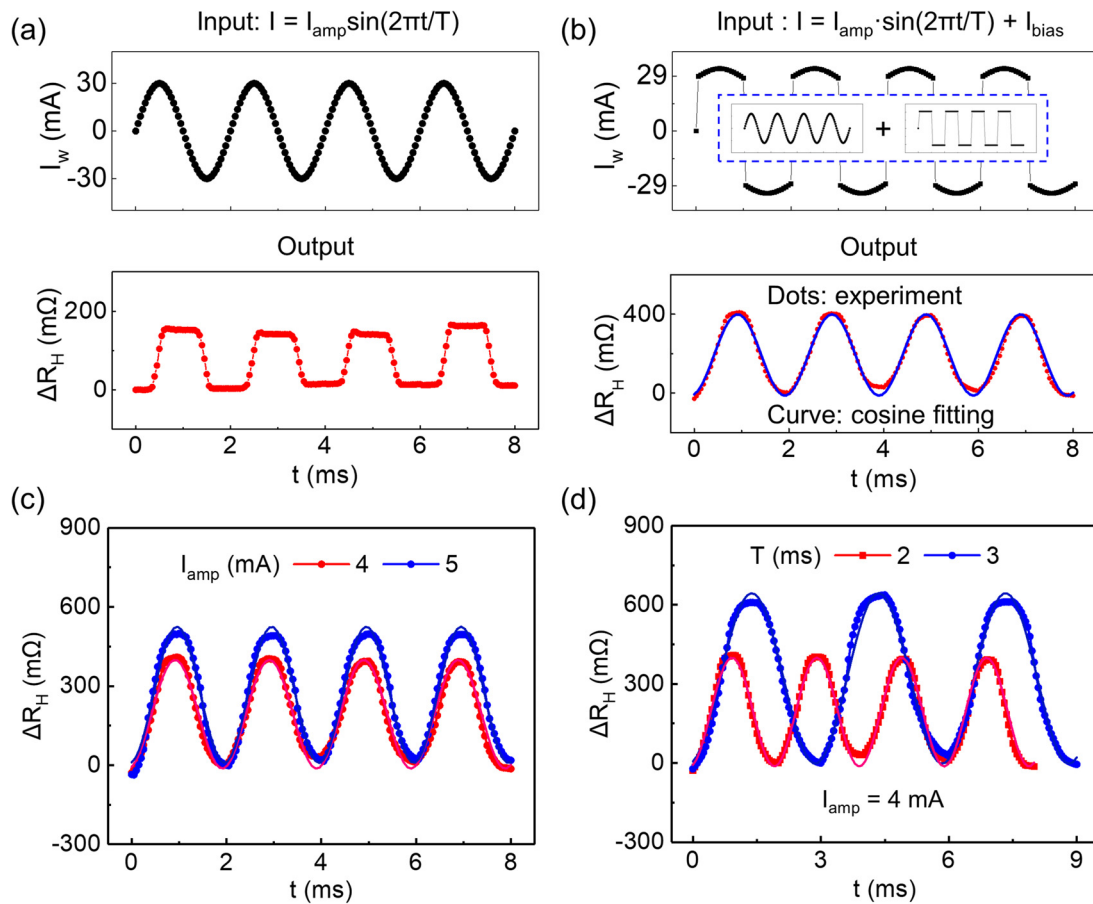


FIG. 4. Input–output characteristic measurement of sine waveform input. (a) Input current of the sine waveform and corresponding output of ΔR_H . The output signal shows a ladder-like waveform rather than a cosine waveform. This visible distortion occurs at stages of I_w smaller than the critical current ($I_c \approx 29$ mA). (b) Input current of the sine waveform along with an assisted bias current (I_{bias}) of a square waveform with amplitude $I_{\text{bias,amp}} = I_c$ and the corresponding output of ΔR_H . (c) and (d) ΔR_H outputs under sine waveform inputs with different I_{amp} (c) and T (d) values.

proven the occurrence of waveform transformation and phase-shift functions. As compared to a traditional RC integrator, the spintronic integrator incurs no leakage error or zero drift originating from the capacitors or op-amps, ensuring a high integral accuracy. Moreover, the output voltage is converted from the resistance and can be simply tuned by tuning the read current. Implementation of the integrator from a single spintronic device will pave the way toward the development of analog electronic elements for beyond-CMOS circuits and also have the potential to be used as the neuromorphic neurons in brain-inspired computing hardware for use in artificial intelligence.

See the [supplementary material](#) for details.

AUTHORS' CONTRIBUTIONS

S.L. and W.T. contributed equally to this work.

The authors acknowledge financial support from the National Natural Science Foundation of China (NSFC Grant Nos. 62074063, 61821003, and 61674062), the National Key Research and

Development Program of China (No. 2020AAA0109000), the Research Project of Wuhan Science and Technology Bureau (No. 2019010701011394), and the Fundamental Research Funds for the Central Universities (HUST: No. 2018KFYXKJC019).

DATA AVAILABILITY

The data that support the findings of this study are available from the corresponding author upon reasonable request.

REFERENCES

- ¹A. Sengupta, Y. Shim, and K. Roy, *IEEE Trans. Biomed. Circuits Syst.* **10**, 1152 (2016).
- ²A. Sengupta and K. Roy, *IEEE Trans. Circuits Syst I* **63**, 2267 (2016).
- ³B. Yu, S. Hu, R. F. Demara, and M. Lin, in *ACM Great Lakes Symposium on VLSI* (2017), pp. 59–64.
- ⁴D. Zhang, X. Yan, E. Zhang, and S. Pan, *Rev. Sci. Instrum.* **87**, 105119 (2016).
- ⁵D. M. Liu, B. N. Wan, Y. Wang, Y. C. Wu, B. Shen, Z. S. Ji, and J. R. Luo, *Rev. Sci. Instrum.* **80**, 053506 (2009).
- ⁶I. M. Miron, K. Garello, G. Gaudin, P. J. Zermatten, M. V. Costache, S. Auffret, S. Bandiera, B. Rodmacq, A. Schuhl, and P. Gambardella, *Nature* **476**, 189 (2011).

- ⁷L. Liu, C. F. Pai, Y. Li, H. W. Tseng, D. C. Ralph, and R. A. Buhrman, *Science* **336**, 555 (2012).
- ⁸D. Bhowmik, L. You, and S. Salahuddin, *Nat. Nanotechnol.* **9**, 59 (2014).
- ⁹G. Yu, P. Upadhyaya, Y. Fan, J. G. Alzate, W. Jiang, K. L. Wong, S. Takei, S. A. Bender, M. Lang, J. Tang, Y. Tserkovnyak, P. K. Amiri, and K. L. Wang, *Nat. Nanotechnol.* **9**, 548 (2014).
- ¹⁰L. You, O. J. Lee, D. Bhowmik, D. Labanowski, J. Hong, J. Bokor, and S. Salahuddin, *Proc. Natl. Acad. Sci. U. S. A.* **112**, 10310 (2015).
- ¹¹S. Fukami, T. Anekawa, C. Zhang, and H. Ohno, *Nat. Nanotechnol.* **11**, 621 (2016).
- ¹²Y. C. Lau, D. Betto, K. Rode, J. M. D. Coey, and P. Stamenov, *Nat. Nanotechnol.* **11**, 758 (2016).
- ¹³K. U. Demasius, T. Phung, W. Zhang, B. P. Hughes, S. H. Yang, A. Kellock, W. Han, A. Pushp, and S. S. P. Parkin, *Nat. Commun.* **7**, 10644 (2016).
- ¹⁴Y. W. Oh, S. H. Chris Baek, Y. M. Kim, H. Y. Lee, K. D. Lee, C. G. Yang, E. S. Park, K. S. Lee, K. W. Kim, G. Go, J. R. Jeong, B. C. Min, H. W. Lee, K. J. Lee, and B. G. Park, *Nat. Nanotechnol.* **11**, 878 (2016).
- ¹⁵K. F. Huang, D. S. Wang, M. H. Tsai, H. H. Lin, and C. H. Lai, *Adv. Mater.* **29**, 1601575 (2017).
- ¹⁶K. Cai, M. Yang, H. Ju, K. W. Edmonds, and K. Wang, *Nat. Mater.* **16**, 712 (2017).
- ¹⁷M. Baumgartner, K. Garello, J. Mendil, C. O. Avci, E. Grimaldi, C. Murer, J. Feng, M. Gabureac, C. Stamm, Y. Acremann, S. Finizio, S. Wintz, J. Raabe, and P. Gambardella, *Nat. Nanotechnol.* **12**, 980 (2017).
- ¹⁸X. Qiu, Z. Shi, W. Fan, S. Zhou, and H. Yang, *Adv. Mater.* **30**, 1705699 (2018).
- ¹⁹W. J. Kong, C. H. Wan, X. Wang, B. S. Tao, L. Huang, C. Fang, C. Y. Guo, Y. Guang, M. Irfan, and X. F. Han, *Nat. Commun.* **10**, 233 (2018).
- ²⁰J. Zhou, X. Wang, Y. Liu, J. Yu, H. Fu, L. Liu, S. I. Chen, J. Deng, W. Lin, X. Shu, H. Y. Yoong, T. Hong, M. Matsuda, P. Yang, S. Adams, B. Yan, X. Han, and J. Chen, *Sci. Adv.* **5**, eaau6696 (2019).
- ²¹R. Mishra, F. Mahfouzi, D. Kumar, K. Cai, M. Chen, X. Qiu, N. Kioussis, and H. Yang, *Nat. Commun.* **10**, 248 (2019).
- ²²N. Sato, F. Xue, R. M. White, C. Bi, and S. X. Wang, *Nat. Electron.* **1**, 508 (2018).
- ²³K. Garello, F. Yasin, H. Hody, S. Couet, L. Souriau, S. H. Sharifi, J. Swerts, R. Carpenter, S. Rao, and W. Kim, in Symposium on VLSI Technology (2019).
- ²⁴S. Zhang, S. Luo, N. Xu, Q. Zou, M. Song, J. Yun, Q. Luo, Z. Guo, R. Li, W. Tian, X. Li, H. Zhou, H. Chen, Y. Zhang, X. Yang, W. Jiang, K. Shen, J. Hong, Z. Yuan, L. Xi, K. Xia, S. Salahuddin, B. Dieni, and L. You, *Adv. Electron. Mater.* **5**, 1800782 (2019).
- ²⁵Y. Cao, A. Rushforth, Y. Sheng, H. Zheng, and K. Wang, *Adv. Funct. Mater.* **29**, 1808104 (2019).
- ²⁶A. Sengupta, Z. Al Azim, X. Fong, and K. Roy, *Appl. Phys. Lett.* **106**, 093704 (2015).
- ²⁷A. Sengupta, A. Banerjee, and K. Roy, *Phys. Rev. Appl.* **6**, 064003 (2016).
- ²⁸K. Obata and G. Tatara, *Phys. Rev. B* **77**, 214429 (2008).
- ²⁹E. Martinez, S. Emori, and G. S. D. Beach, *Appl. Phys. Lett.* **103**, 072406 (2013).
- ³⁰S. H. Yang, K. S. Ryu, and S. Parkin, *Nat. Nanotechnol.* **10**, 221 (2015).
- ³¹M. Yamanouchi, D. Chiba, F. Matsukura, T. Dietl, and H. Ohno, *Phys. Rev. Lett.* **96**, 096601 (2006).
- ³²A. Thiaville, Y. Nakatani, J. Miltat, and Y. Suzuki, *Europhys. Lett.* **69**, 990 (2005).
- ³³T. Suzuki, H. Tanigawa, Y. Kobayashi, K. Mori, and H. Ohno, in Symposium on VLSI Technology (2013).
- ³⁴S. Fukami, T. Suzuki, Y. Nakatani, N. Ishiwata, and H. Ohno, *Appl. Phys. Lett.* **98**, 082504 (2011).
- ³⁵P. P. J. Haazen, E. Murè, J. H. Franken, R. Lavrijsen, H. J. M. Swagten, and B. Koopmans, *Nat. Mater.* **12**, 299 (2013).
- ³⁶O. Boulle, S. Rohart, L. D. Buda-Prejbeanu, E. Jue, I. M. Miron, S. Pizzini, J. Vogel, G. Gaudin, and A. Thiaville, *Phys. Rev. Lett.* **111**, 217203 (2013).
- ³⁷K. S. Ryu, L. Thomas, S. H. Yang, and S. S. P. Parkin, *Appl. Phys. Express* **5**, 093006 (2012).
- ³⁸S. Emori, U. Bauer, S. M. Ahn, E. Martinez, and G. S. D. Beach, *Nat. Mater.* **12**, 611 (2013).